Supplemental Material for

Aberrant activation of p53/p66Shc-mInsc axis increases asymmetric divisions and attenuates proliferation of aged mammary stem cells

Chiara Priami[1,6], Daniela Montariello[1,6], Giulia De Michele[1], Federica Ruscitto[1], Andrea Polazzi[1], Simona Ronzoni[1], Giovanni Bertalot[1,2], Giorgio Binelli[3], Valentina Gambino[1,5], Lucilla Luzi[1], Marina Mapelli[1], Marco Giorgio[1,4], Enrica Migliaccio[1,7] and Pier Giuseppe Pelicci[1,5,7]

[1]European Institute of Oncology (IEO) IRCCS, Via Ripamonti 435, 20141 Milan, Italy

[2]U.O.M. Anatomia ed Istologia Patologica, Ospedale Santa Chiara, Largo Medaglie d'Oro 9, 38122 Trento, Italy

[3]Department of Biotechnology and Life Sciences, University of Insubria, Via Dunant 3, 21100 Varese, Italy

[4]Department of Biomedical Sciences, University of Padua, Via Bassi 58/B, 35131 Padova, Italy

[5]Department of Oncology and Hemato-Oncology, University of Milan, Via Santa Sofia 9, 20142 Milan, Italy

[6]These authors contributed equally to this work.

[7]Corresponding authors.

To whom correspondence should be addressed:

E.M.: enrica.migliaccio@ieo.it; phone: +390294372198;

P.G.P.: piergiuseppe.pelicci@ieo.it; phone: +390257489831

The authors declare no potential conflict of interests.

Supplemental Figures

Figure S1

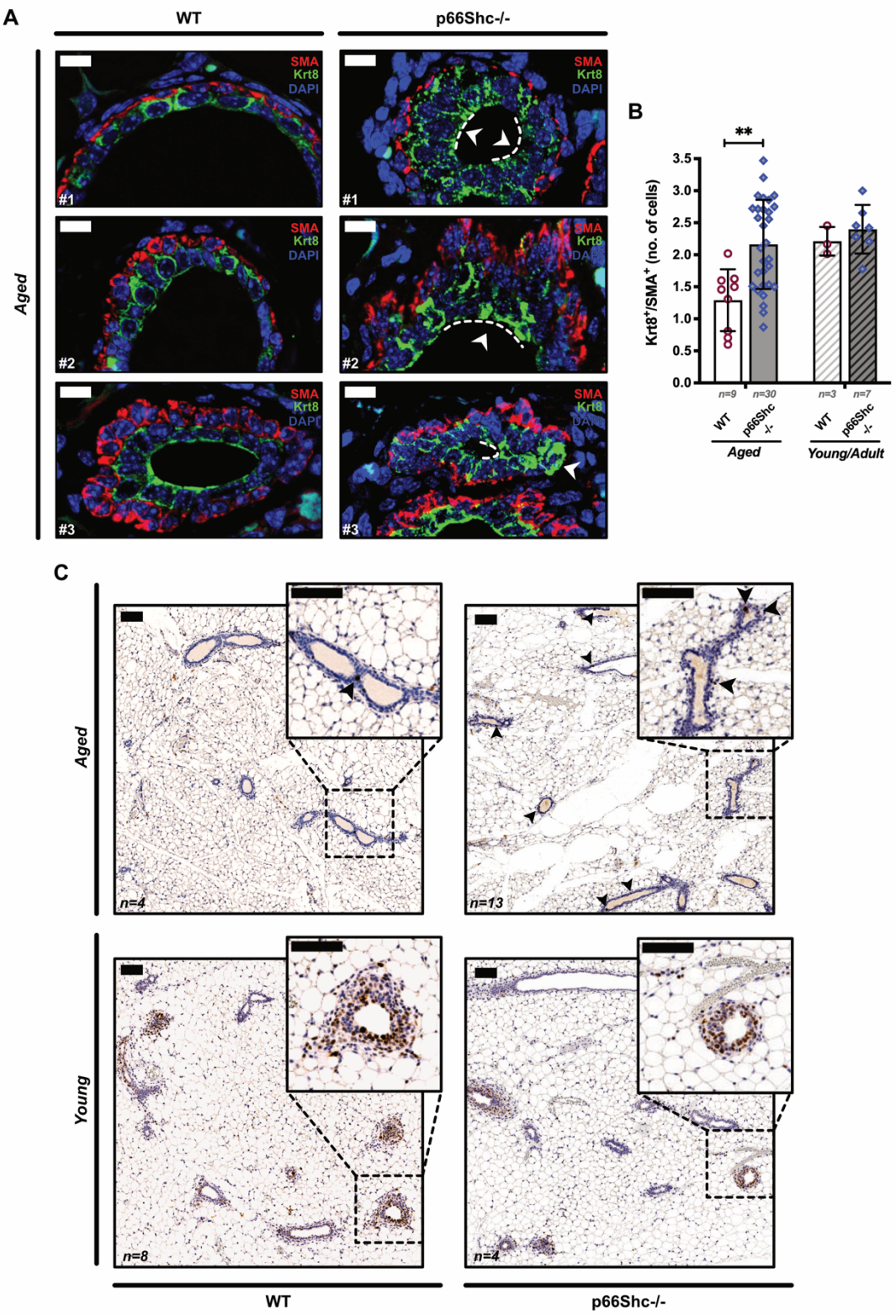

Figure S1. Increased proliferation of ductal luminal epithelium in aged p66Shc-/- mammary glands (MGs). **(A)** Representative confocal images of immunofluorescence analysis of basal (SMA^+, red) and luminal ($Krt8^+$, green) epithelia in aged WT (*n*=3) or p66Shc-/- (*n*=5) MGs (same experiment as in Figure 2D). White arrow-heads and dashed lines indicate areas of luminal hyperplasia. Nuclei are stained by DAPI (blue). Scale bar=10μm. **(B)** Quantification of increased cellularity within the luminal epithelium in aged p66Shc-/- MGs, expressed as the ratio of $Krt8^+$-cells to SMA^+-cells (same experiment as in A and Figure 2D). Numbers of analyzed ducts/lobules are indicated. Data are analyzed by 2-way ANOVA and Tukey *post-hoc* test; **: *P*=0.0028. **(C)** Representative images of Ki67 immunohistochemistry analysis in MGs from aged (24-mo-old) WT (*n*=4) or p66Shc-/- (*n*=13) and young (2-mo-old) WT (*n*=8) or p66Shc-/- (*n*=4) mice (same experiment as in Figure 2E). Scale bar=100μm; arrow-heads: $Ki67^+$-cells. In each panel, the area marked by the black dashed line is shown at higher magnification.

Figure S2

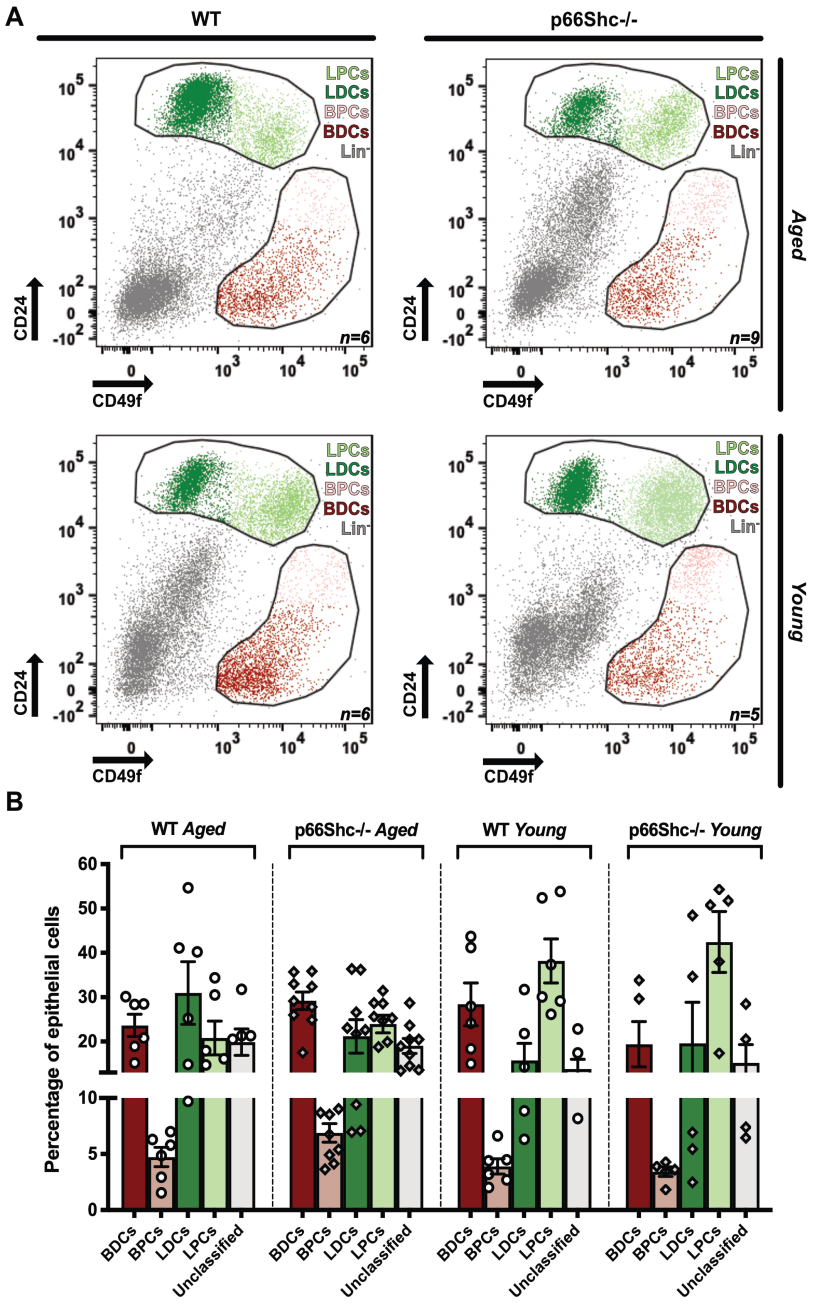

Figure S2. Similar frequencies of basal and luminal progenitor cells in aged* vs *young WT or p66Shc-/- mammary glands (MGs). **(A)** Representative dot-plots obtained by FACS-analysis of primary mammary epithelial cells from aged WT (*n*=6) or p66Shc-/- (*n*=9) and young WT (*n*=6) or p66Shc-/- (*n*=5) mice. Lin$^-$ cells (gray) are gated as follows: CD24^{hi}CD49f^{med}: luminal progenitors (LPCs, light green); CD24^{hi}CD49f$^{lo/neg}$: luminal differentiated cells (LCDs, dark green); CD24^{med}CD49f^{hi}: basal progenitors (BPCs, light red); CD49f$^{med/hi}$CD24$^{lo/neg}$: basal differentiated cells (BDCs, dark red). **(B)** Percentages of epithelial cell-subpopulations depicted in (A). Epithelial cells not assigned to any category are shown in gray (Unclassified). Data are represented as mean±SEM. 2-way ANOVA reveals no significant difference between ages or genotype.

Figure S3

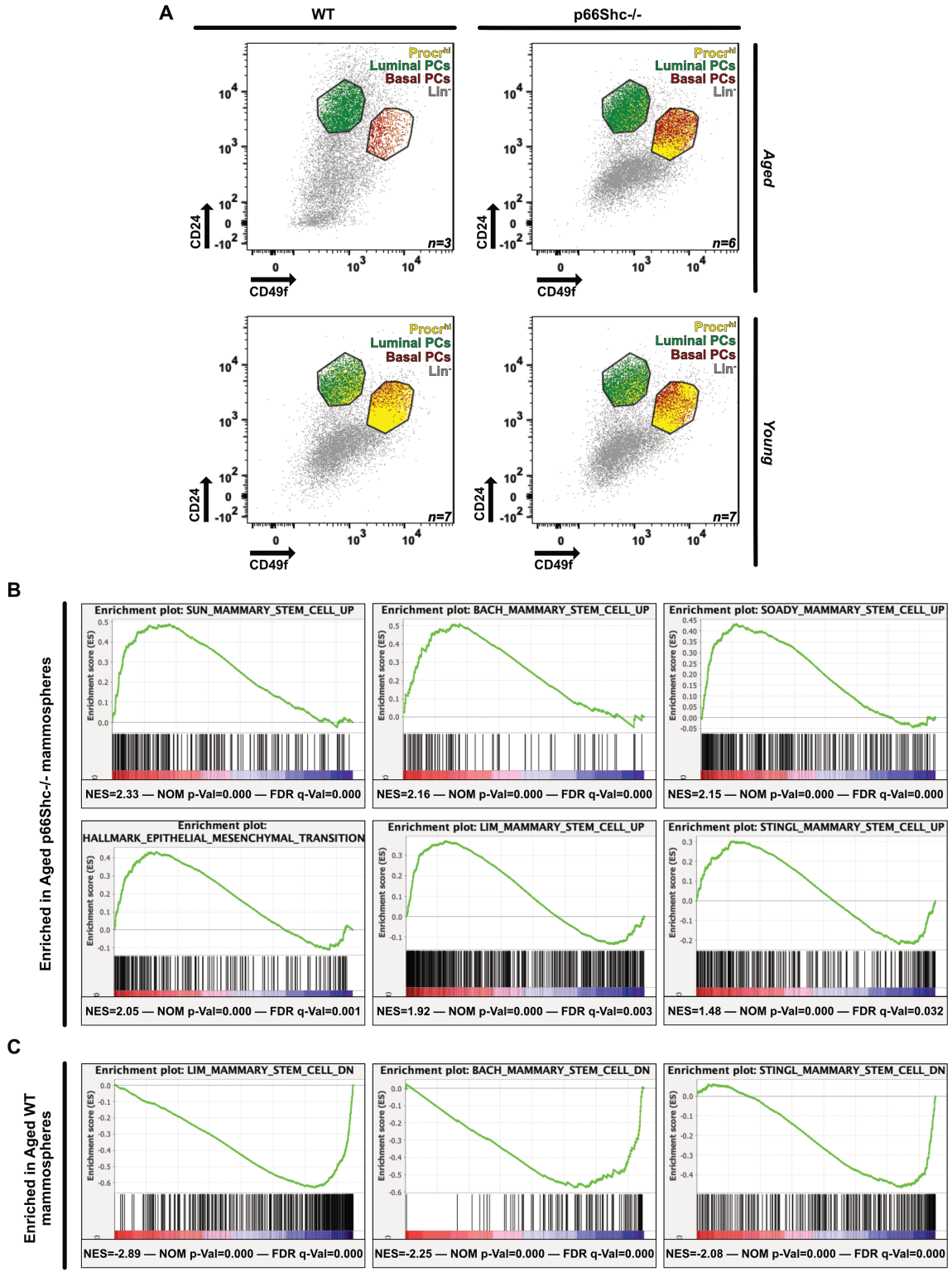
A
WT
p66Shc-/-
Procr^hi
Luminal PCs
Basal PCs
Lin-
CD24
CD49f
n=3
n=6
n=7
n=7
Aged
Young
B
Enriched in Aged p66Shc-/- mammospheres
Enrichment plot: SUN_MAMMARY_STEM_CELL_UP
NES=2.33 — NOM p-Val=0.000 — FDR q-Val=0.000
Enrichment plot: BACH_MAMMARY_STEM_CELL_UP
NES=2.16 — NOM p-Val=0.000 — FDR q-Val=0.000
Enrichment plot: SOADY_MAMMARY_STEM_CELL_UP
NES=2.15 — NOM p-Val=0.000 — FDR q-Val=0.000
Enrichment plot: HALLMARK_EPITHELIAL_MESENCHYMAL_TRANSITION
NES=2.05 — NOM p-Val=0.000 — FDR q-Val=0.001
Enrichment plot: LIM_MAMMARY_STEM_CELL_UP
NES=1.92 — NOM p-Val=0.000 — FDR q-Val=0.003
Enrichment plot: STINGL_MAMMARY_STEM_CELL_UP
NES=1.48 — NOM p-Val=0.000 — FDR q-Val=0.032
C
Enriched in Aged WT mammospheres
Enrichment plot: LIM_MAMMARY_STEM_CELL_DN
NES=-2.89 — NOM p-Val=0.000 — FDR q-Val=0.000
Enrichment plot: BACH_MAMMARY_STEM_CELL_DN
NES=-2.25 — NOM p-Val=0.000 — FDR q-Val=0.000
Enrichment plot: STINGL_MAMMARY_STEM_CELL_DN
NES=-2.08 — NOM p-Val=0.000 — FDR q-Val=0.000

Figure S3. Increased expression of mammary stem cell (MaSC) markers in aged p66Shc-/- mammospheres. **(A)** Representative dot-plots obtained by FACS-analysis of M2-mammosphere cell suspensions from aged or young WT or p66Shc-/- mice (same experiment as in Figure 3A). Numbers of independent preparations are indicated. Lin^- cells (gray) are gated as follows: $CD24^{hi}CD49f^{med}$: luminal progenitors (Luminal PCs, green) and $CD24^{med}CD49f^{hi}$: basal progenitors (Basal PCs, red); $Procr^{hi}$-subpopulations are depicted in yellow. **(B,C)** Enrichment plots obtained by Gene Set Enrichment Analysis (30) of aged p66Shc-/- *vs* WT mammospheres, analyzed by bulk RNA-sequencing. Raw expression levels were compared for enrichment in gene sets-listed in Dataset 1 (same experiment as in Figure 3C-D). Top-enriched, MaSC-related datasets in aged p66Shc-/- (B) or WT (C) mammospheres are shown. Normalized enrichment scores (NES), nominal *P* values (NOM p-Val) and false discovery rates (FDR q-Val) are indicated.

Figure S4

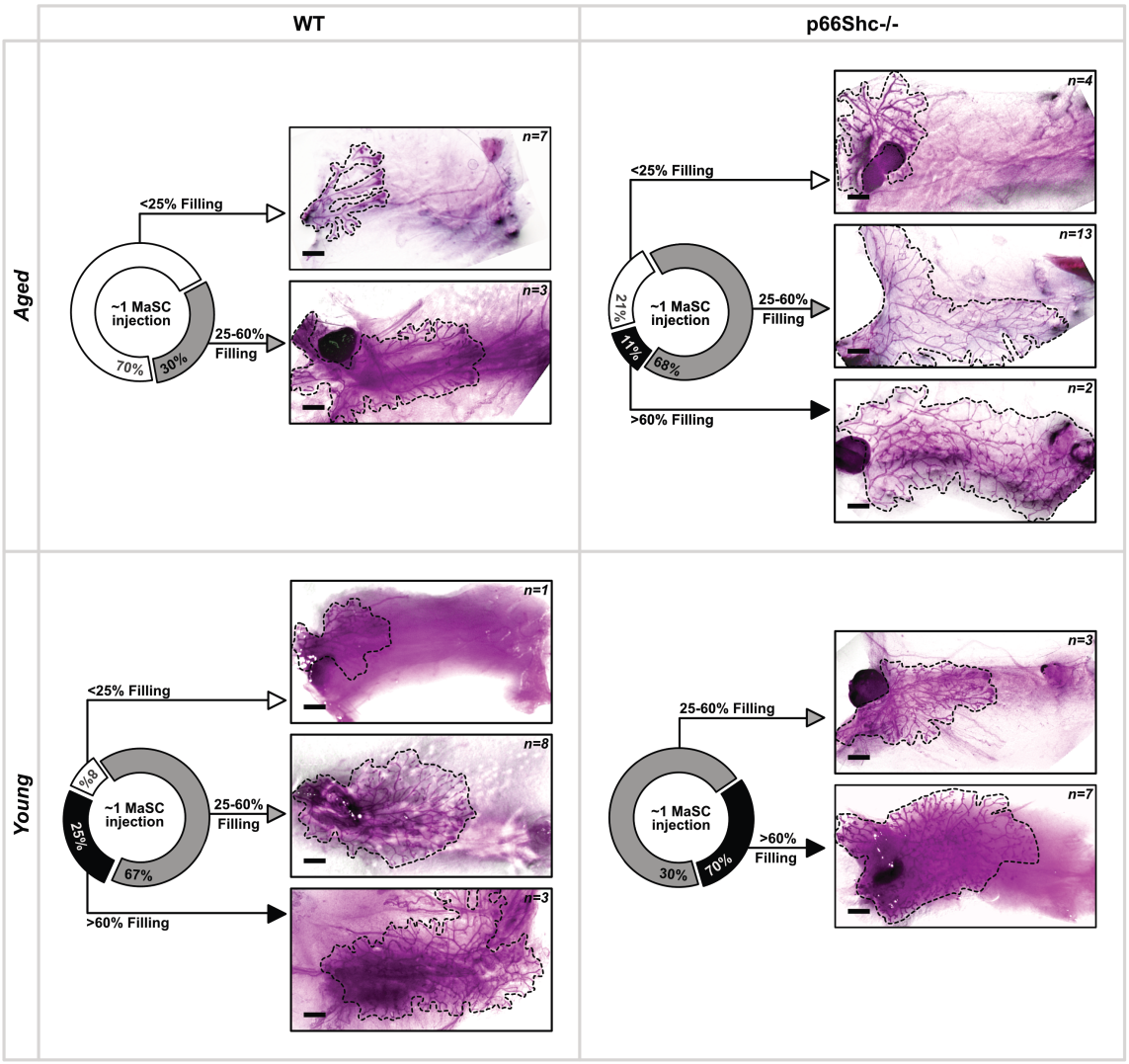

Figure S4. Increased regenerative potential of aged p66Shc-/- MaSCs. Representative carmine-stained whole-mount images of outgrowths obtained upon heterochronic transplantation of rate-limiting diluted M2-mammosphere cell suspensions from aged and young, WT or p66Shc-/- mice, into the cleared fat-pads of syngeneic 3-week-old mice. Outgrowths obtained with ~1 MaSC were categorized as filling <25%, 25%-60% or >60% of recipient's fat-pad area. Examples for each category are shown, together with donut-charts depicting percentages of outgrowths obtained for each category. Outgrowths are outlined. Scale bar:1mm.

Figure S5

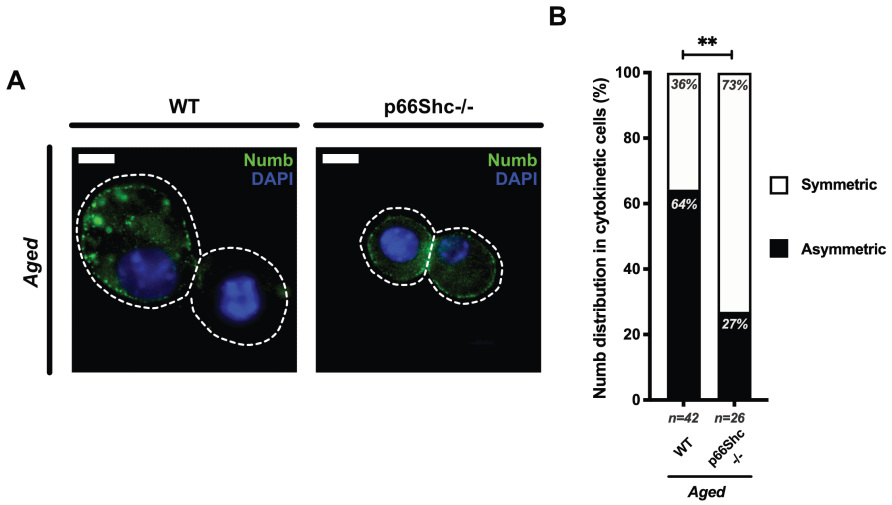

Figure S5. Increased symmetric distribution of Numb in aged p66Shc-/- mammospheres. **(A)** Numb distribution in cytokinetic cell-doublets, obtained after plating single-cell suspensions of M2-mammospheres from aged WT or p66Shc-/- mice ($n \geq 3$ for each preparation). Numb (green) is either asymmetrically or symmetrically distributed. Cells and cleavage sites are outlined. Nuclei are shown by DAPI (blue). Scale bar=10μm. **(B)** Frequencies of either asymmetrical (black) or symmetrical (white) distribution of Numb in cytokinetic cell-doublets. Numbers of scored doublets are indicated. Statistical analysis: Chi-square test with Yates' correction. **: P=0.006.

Figure S6

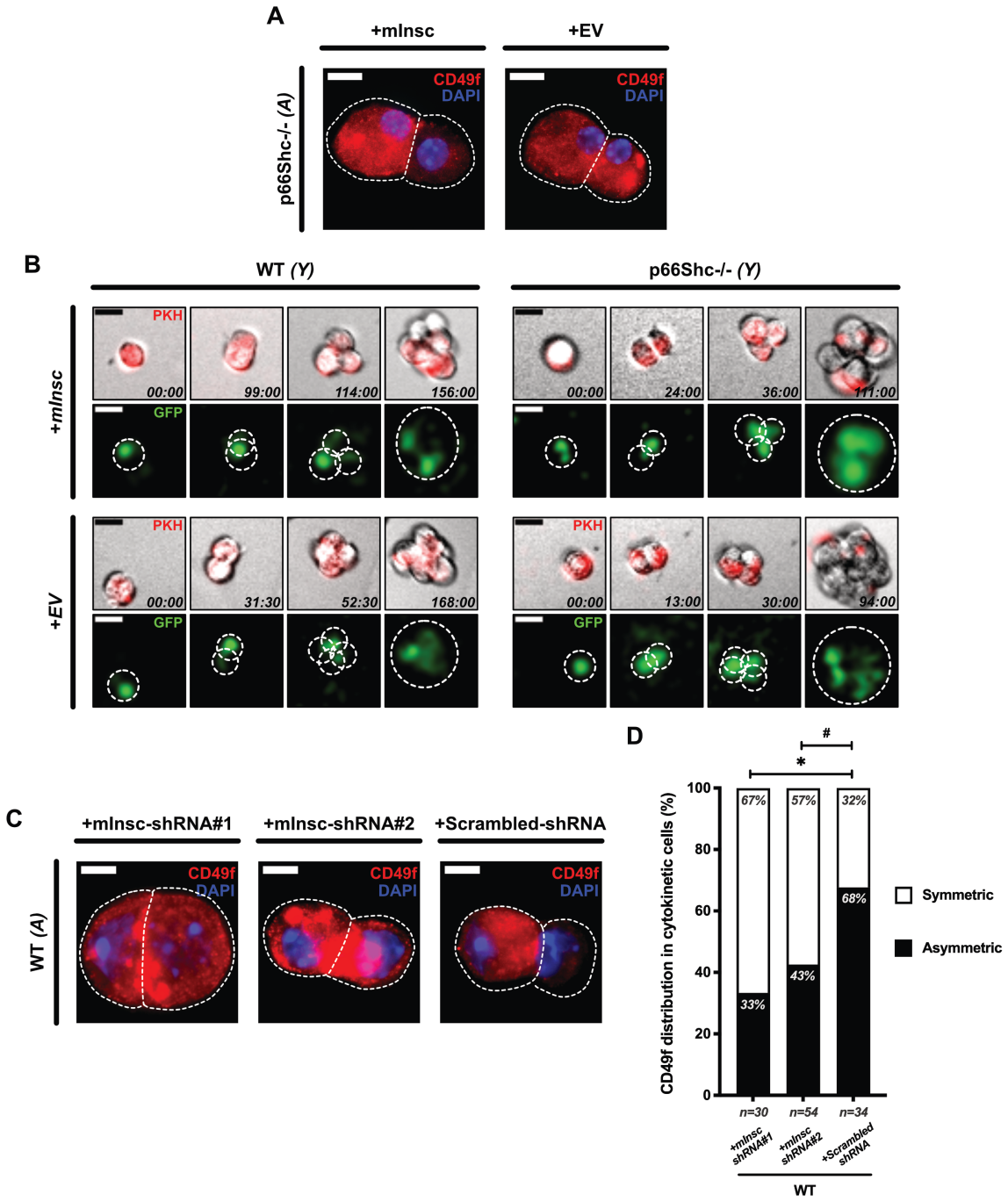

Figure S6. mInsc-overexpression restores asymmetric divisions of p66Shc-/- mammary stem cells (MaSCs), while mInsc-knockdown prevents asymmetric divisions of aged WT MaSCs. **(A,C)** CD49f distribution in cytokinetic cell-doublets obtained after plating single-cell suspensions of M2-mammospheres from aged p66Shc-/- (A) mice or aged WT (C) mice ($n \geq 3$ for each preparation). In A, cells were infected with either mInsc-overexpressing- (*+mInsc*) or empty- (*+EV*) lentiviral vectors. In C, cells were infected with two anti-mInsc shRNA vectors (*+mInsc-shRNA#1* and *-#2*) or control-vector (*+Scrambled-shRNA*). In both A and C, CD49f (red) is either

asymmetrically or symmetrically distributed. Cells and cleavage sites are outlined. Nuclei are shown by DAPI (blue). Scale bar=10µm. **(B)** Time-lapse microscopy of $PKH^{+}GFP^{+}$-cells from M2-mammosphere cell suspensions. Mammospheres from aged and young WT or p66Shc-/- mice (*n*≥3 for each preparation) were infected with either mInsc-overexpressing- (+*mInsc*) or empty- (+*EV*) vectors. Early and late time-points are shown. Shooting-times are indicated as *hours:minutes*. Cells and spheroids are outlined. Scale bar=20µm. **(D)** Frequencies of either asymmetrical (black) or symmetrical (white) CD49f distribution in mInsc-knocked down aged WT MaSCs (same experiment as in C). Numbers of scored cell-doublets are indicated. Statistical analysis: pairwise Chi-square test with Yates' correction. *****: *P*=0.013; **#**: *P*=0.038.

Figure S7

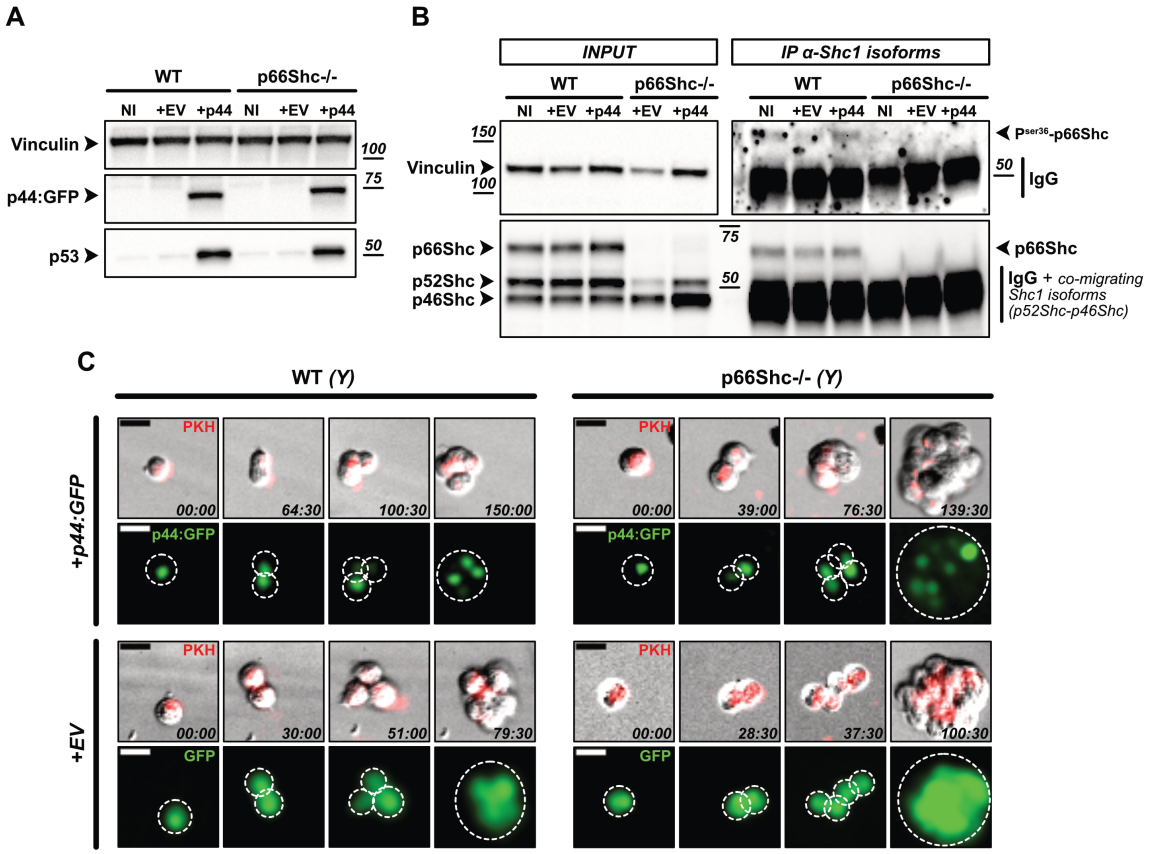

Figure S7. p44 stabilizes p53, activates p66Shc, induces asymmetric division and decreases proliferation of mammary stem cells (MaSCs). **(A)** Western blot (WB) on not-infected (*NI*), control-infected (*+EV*) and p44:GFP-infected (*+p44*) WT and p66Shc-/- primary mammary epithelial cells. p66Shc-independent expression of p44:GFP fusion protein (middle panel) and p53 stabilization in p44:GFP-infected cells (lower panel) are readily detectable. Vinculin is used as a loading control. **(B)** WB of input (left) and immunoprecipitated (IP, right) lysates from not-infected (*NI*), control-infected (*+EV*) and p44:GFP-infected (*+p44*) WT and p66Shc-/- primary mammary epithelial cells. Immunoprecipitation was performed with an anti-Shc1 antibody, which binds to all the Shc1 isoforms (p66Shc, p52Shc and p46Shc, as indicated in the input). WB of IPs shows modest activation of p66Shc (P^{ser36}-p66Shc, upper-right panel) upon p44:GFP-overexpression. Vinculin is used a as loading control. **(C)** Time-lapse microscopy of $PKH^{+}GFP^{+}$-cells from M2-mammosphere cell suspensions. Mammospheres from young WT or p66Shc-/- mice ($n \geq 3$ mice for each preparation) were infected with either p44:GFP-expressing- (*+p44:GFP*) or empty- (*+EV*) vectors. Early and late time-points are shown. Shooting-times are indicated as *hours:minutes*. Cells and spheroids are outlined. Note nuclear localization of p44:GFP. Scale bar=20μm.

Supplementary Tables

Table S1

	No. of transplanted cells (experimental)	No. of MaSCs (inferred)	Aged donors						
			No. of injected mice	Outgrowth extension (% of fat pad area) 100-81	80-61	60-41	40-26	26-15	Total
WT donors	**50 000**	*100 ≳ n ≳ 30*	9	0	1	4	2	2	9
	5 000	*10 ≳ n ≳ 3*	10	0	1	5	1	3	10
	2 000	*3 ≳ n ≳ 1*	3	0	0	0	0	2	2
	1 000	*n ≈ 1*	3	0	0	0	0	1	1
	500	*n ≲ 1*	21	0	0	1	2	2	5
	100	*n ≲ 1*	11	0	0	0	0	2	2
	50	*n ≲ 1*	10	0	0	0	0	0	0
	25	*n ≲ 1*	10	0	0	0	0	0	0
		Total	**77**	0	2	10	5	12	**29**
			Estimated MaSC frequency for Aged WT = 1:1 507						
			Limits: lower = 1:2 520 - upper = 1:901						
p66Shc-/- donors	**50 000**	*100 ≳ n ≳ 30*	9	4	1	3	1	0	9
	5 000	*10 ≳ n ≳ 3*	8	4	1	2	1	0	8
	2 000	*3 ≳ n ≳ 1*	4	0	0	2	0	2	4
	1 000	*n ≈ 1*	3	0	0	1	0	1	2
	500	*n ≲ 1*	20	0	1	2	3	2	8
	100	*n ≲ 1*	15	0	1	3	3	0	7
	50	*n ≲ 1*	10	0	0	1	0	1	2
	25	*n ≲ 1*	8	0	0	0	0	0	0
		Total	**77**	8	4	14	8	6	**40**
			Estimated MaSC frequency for Aged p66Shc-/- = 1:577						
			Limits: lower = 1:916 - upper = 1:364						

	No. of transplanted cells (experimental)	No. of MaSCs (inferred)	Young donors						
			No. of injected mice	Outgrowth extension (% of fat pad area) 100-81	80-61	60-41	40-26	26-15	Total
WT donors	**50 000**	*100 ≳ n ≳ 30*	16	1	3	9	3	0	16
	5 000	*10 ≳ n ≳ 3*	12	0	5	4	2	1	12
	500	*n ≈ 1*	14	0	3	2	2	0	7
	100	*n ≲ 1*	10	0	0	0	4	1	5
	50	*n ≲ 1*	6	0	0	0	0	0	0
	25	*n ≲ 1*	6	0	0	0	0	0	0
		Total	**64**	1	11	15	11	2	**40**
			Estimated SC frequency for Young WT = 1:514						
			Limits: lower = 1:934 - upper = 1:283						
p66Shc-/- donors	**50 000**	*100 ≳ n ≳ 30*	8	2	2	3	1	0	8
	5 000	*10 ≳ n ≳ 3*	4	0	2	2	0	0	4
	500	*n ≈ 1*	8	1	0	3	0	0	4
	100	*n ≲ 1*	8	0	0	4	0	0	4
	50	*n ≲ 1*	8	1	1	0	0	0	2
	25	*n ≲ 1*	8	0	0	0	0	0	0
		Total	**44**	4	5	12	1	0	**22**
			Estimated SC frequency for Young p66Shc-/- = 1:393						
			Limits: lower = 1:778 - upper = 1:200						

Table S1. Increased number of mammary stem cells (MaSCs) in mammospheres from aged p66Shc-/- mice. Limiting-dilution heterochronic transplantation of M2-mammosphere cell suspensions from aged and young, WT or p66Shc-/- mice, into the cleared fat-pads of 3-week-old syngeneic recipients. Recipient mice were categorized by outgrowth extension, calculated as percentage of repopulated fat-pad area. Outgrowths filling less than 15% were considered as unsuccessful engraftments. Numbers of transplanted cells, inferred numbers of transplanted MaSCs (=no. of transplanted cells/estimated MaSC frequency), numbers of injected mice and obtained outgrowths are indicated, as well as estimated MaSC frequencies and confidence intervals. MaSC frequencies and statistical differences between groups were calculated pairwise with ELDA (63): P=0.006 for Aged WT *vs* Aged p66Shc-/- groups; P=0.009 for Aged WT *vs* Young WT groups; other comparisons yielded not significant results.

Table S2

			Dividing PKH+/GFP+ cells								
	Modality of division		*Asymmetric cell divisions*				*Symmetric cell divisions*				*Total no. of observed cells*
	Rounds of division		*2*	*3*	*>3*	*Total ACD*	*2*	*3*	*>3*	*Total SCD*	
Aged	**WT +*EV***	*No. of cells*	48	47	6	101	16	8	1	25	126
		%	**48**	**47**	**6**		**64**	**32**	**4**		
	p66Shc-/- +*EV*	*No. of cells*	12	11	10	33	8	14	11	33	66
		%	**36**	**33**	**30**		**24**	**42**	**33**		
Young	**WT +*EV***	*No. of cells*	56	59	19	134	40	41	20	101	235
		%	**42**	**44**	**14**		**40**	**41**	**20**		
	p66Shc-/- +*EV*	*No. of cells*	40	43	14	97	25	64	40	129	226
		%	**41**	**44**	**14**		**19**	**50**	**31**		
	p66Shc-/- +*p66Shc*	*No. of cells*	48	32	6	86	10	20	2	32	118
		%	**56**	**37**	**7**		**31**	**63**	**6**		

Table S2. p66Shc-/- deletion promotes mammary stem cell (MaSC) proliferation, regardless of their modality of division. PKH^+GFP^+-M2-mammosphere cells from young and aged, WT or p66Shc-/- mice were observed by 7-day time-lapse imaging to score asymmetric *vs* symmetric divisions and rounds of divisions entered. MaSCs were categorized according to their modality of division (ACD or SCD) and sub-categorized by rounds of division entered (2, 3 or >3). Numbers and percentages of cells are indicated for each group. For "Aged WT *+EV*", "Aged p66Shc-/- *+EV*" and "Young p66Shc-/- *+p66Shc*" groups, MaSCs were the same of experiments depicted in Fig. 5C-E. For "Young WT *+EV*" and "Young p66Shc-/- *+EV*" groups, MaSCs were pooled from experiments depicted in Figures 5C-E and 7A,C. Chi-square test reveals no significant difference between asymmetrically- and symmetrically- dividing MaSCs in rounds of division entered.

Table S3

		Aged						*Young*					
		WT			p66Shc-/-			WT			p66Shc-/-		
Gene symbol	**Category**	**FC**	**SEM(FC)**	**N**	**FC**	**SEM(FC)**	**N**	**FC**	**SEM(FC)**	**N**	**FC**	**SEM(FC)**	**N**
Aldh1a1	MaSC marker	-1.607	0.043	3	1.195	0.416	3	1.000	0.047	6	-1.098	0.182	8
Anapc5	Cell cycle	-1.362	0.025	3	1.145	0.162	3	1.000	0.116	3	1.234	0.126	3
Anln	Cell cycle	-3.159	0.113	3	-2.861	0.078	3	1.000	0.005	3	-1.008	0.081	3
Aurka	Cell cycle/polarity	-2.361	0.057	3	-3.746	0.043	3	1.000	0.047	3	1.054	0.268	3
Aurkb	Cell cycle/polarity	-2.758	0.008	3	-2.928	0.033	3	1.000	0.009	3	1.001	0.234	3
Bub1	Cell cycle	-3.196	0.023	3	-1.880	0.064	3	1.000	0.014	3	1.148	0.151	3
Bub1b	Cell cycle	-2.687	0.142	3	-2.827	0.040	3	1.000	0.266	3	1.061	0.223	3
Bub3	Cell cycle	-1.893	0.050	3	-1.365	0.097	3	1.000	0.231	3	-1.427	0.082	3
Ccna2	Cell cycle	-6.404	0.017	3	-2.910	0.042	3	1.000	0.129	3	-1.049	0.257	3
Ccnb1	Cell cycle	-3.152	0.028	3	-3.040	0.049	3	1.000	0.073	3	1.017	0.141	3
Ccnb2	Cell cycle	-2.327	0.060	3	-3.156	0.044	3	1.000	0.021	3	-1.114	0.197	3
Ccnf	Cell cycle	-2.328	0.010	3	-4.274	0.018	3	1.000	0.012	3	-1.037	0.176	3
Cdc20	Cell cycle	-2.516	0.072	3	-4.350	0.047	3	1.000	0.026	3	1.353	0.196	3
Cdca2	Cell cycle	-2.708	0.044	3	-3.478	0.022	3	1.000	0.140	3	-1.075	0.106	3
Cdk1	Cell cycle	-3.962	0.117	3	-2.037	0.117	3	1.000	0.174	3	1.258	0.356	3
Cdk2	Cell cycle	-1.309	0.063	3	-1.736	0.013	3	1.000	0.098	3	-1.214	0.065	3
Cenpe	Cell cycle	-2.793	0.061	3	-2.797	0.036	3	1.000	0.011	3	1.101	0.141	3
Chek1	Cell cycle	-2.391	0.032	3	-1.629	0.059	3	1.000	0.009	3	1.004	0.087	3
Haus2	Cell cycle	1.024	0.033	3	1.126	0.236	3	1.000	0.072	3	1.381	0.473	3
Incenp	Cell cycle	-2.059	0.016	3	-1.725	0.053	3	1.000	0.019	3	-1.010	0.128	3
Kif20a	Cell cycle	-2.517	0.051	3	-3.460	0.086	3	1.000	0.121	3	1.168	0.214	3
Kif2c	Cell cycle	-2.807	0.011	3	-4.617	0.033	3	1.000	0.034	3	-1.446	0.020	3
LGN (Gpsm2)	Cell polarity	-1.558	0.048	3	-1.538	0.047	3	1.000	0.234	3	1.100	0.079	3
Mad2l1	Cell cycle	-2.295	0.093	3	-2.623	0.044	3	1.000	0.086	3	-1.081	0.044	3
mInsc (Insc)	Cell polarity	1.074	0.129	3	-5.355	0.082	3	1.000	0.184	6	-1.195	0.165	8
Mis12	Cell cycle	-2.831	0.046	3	-1.526	0.091	3	1.000	0.606	3	-1.398	0.027	3
Mphosph8	Cell cycle	-1.157	0.072	3	-1.511	0.017	3	1.000	0.152	3	-1.288	0.078	3
Ncapd2	Cell cycle	-2.314	0.024	3	-3.037	0.087	3	1.000	0.157	3	-1.141	0.145	3
NuMA (Numa1)	Cell polarity	1.430	0.113	3	1.404	0.402	3	1.000	0.121	3	1.402	0.151	3
Numb	Cell polarity	1.581	0.123	3	1.089	0.134	3	1.000	0.030	3	-1.241	0.183	3
Par3 (Pard3)	Cell polarity	1.361	0.164	3	1.258	0.078	3	1.000	0.004	3	-1.329	0.115	3
Par6 (Pard6a)	Cell polarity	1.435	0.142	3	-1.607	0.121	3	1.000	0.221	6	-1.776	0.141	6
Plk1	Cell cycle/polarity	-2.603	0.029	3	-3.483	0.068	3	1.000	0.167	3	1.208	0.164	3
Plk4	Cell cycle/polarity	-1.946	0.033	3	-1.312	0.068	3	1.000	0.088	3	1.173	0.170	3
Smc4	Cell cycle	-1.490	0.024	3	-1.967	0.068	3	1.000	0.063	3	-1.402	0.075	3
Spag5 (Astrin)	Cell cycle	-2.964	0.020	3	-3.361	0.055	3	1.000	0.039	3	1.042	0.048	3
Top2a	Cell cycle	-2.330	0.085	3	-2.844	0.034	3	1.000	0.191	3	-1.282	0.141	3

Table S3. qRT-PCR expression levels of genes analyzed in the present study. Mean qRT-PCR expression levels are shown as fold-changes (FCs) over "young WT" values, used as calibrators. 0<FCs<1 are expressed as -1/FC (negative FCs). SEM (standard error of the mean) and N (sample size) are indicated.

Table S4

Antibody	Source	Identifier	Working dilution	Application
Mouse monoclonal **anti-(a-Smooth-Muscle Actin**), clone 1A4	Agilent Technologies, Santa Clara, CA, USA	Cat#M0851	1:150	Immunofluorescence on FFPE tissues
Rabbit polyclonal **anti-(Cytokeratin-8)**	Abcam, Cambridge, Cambs, UK	Cat#ab59400	1:200	Immunofluorescence on FFPE tissues
Rabbit monoclonal **anti-Ki67**, clone SP6	Thermo Fisher Scientific, Waltham, MA, USA	Cat#MA5-14520	1:200	Immunohistochemistry on FFPE tissues
Rat monoclonal **anti-CD45**, clone 30-F11, PE-Cy7 conjugated	Thermo Fisher Scientific	Cat#25-0451-82	1:300	Flow cytometry
Rat monoclonal **anti-CD31** (PECAM-1), clone 390, PE-Cy7 conjugated	Thermo Fisher Scientific	Cat#25-0311-82	1:300	Flow cytometry
Rat monoclonal **anti-(TER-119)**, clone TER-119, PE-Cy7 conjugated	Thermo Fisher Scientific	Cat#25-5921-81	1:300	Flow cytometry
Rat monoclonal **anti-CD24**, clone M1/69, PE-conjugated	Thermo Fisher Scientific	Cat#12-0242-82	1:200	Flow cytometry
Rat monoclonal **anti-CD49f** (Integrin a6), clone GoH3, FITC-conjugated	Thermo Fisher Scientific	Cat#11-0495-82	1:100	Flow cytometry
Rat monoclonal **anti-CD49f** (Integrin a6), clone GoH3, APC-conjugated	Thermo Fisher Scientific	Cat#17-0495-82	1:100	Flow cytometry
Rat monoclonal **anti-CD201 (EPCR)**, clone 1560, APC-conjugated	Thermo Fisher Scientific	Cat#17-2012-82	1:100	Flow cytometry
Rat monoclonal **anti-CD49f** (Integrin a6), clone GoH3	BD Biosciences, Franklin Lakes, NJ, USA	Cat#555734	1:200	Immunocytofluorescence
Mouse monoclonal **anti-Numb**, clone AB21	Pier Paolo Di Fiore Lab; Colaluca *et al.*, 2008	N/A	1:1 000	Immunocytofluorescence
Mouse monoclonal **anti-p53**, clone 1C12	Cell Signaling Technology (CST), Danvers, MA, USA	Cat#2524	1:1 000	Western blot
Rabbit polyclonal **anti-Shc1**	BD Biosciences	Cat#610081	1:1 000	Western blot, Immunoprecipitation
Mouse monoclonal **anti-(phospho-Ser36-p66Shc)**, clone 6E10	Enzo Life Sciences, Farmingdale, NY, USA	Cat#ALX-804-358-C100	1:200	Western blot
Rabbit polyclonal **anti-GFP**	Abcam	Cat#ab290	1:1 000	Western blot
Mouse monoclonal **anti-Vinculin**, clone hVin-1	Merck, Darmstadt, HE, Germany	Cat#V9131	1:20 000	Western blot
Donkey polyclonal **anti-(Mouse-IgG)**, Cy3-conjugated	Jackson ImmunoResearch, West Grove, PA, USA	Cat#715-165-150	1:400	Immunofluorescence
Donkey polyclonal **anti-(Mouse-IgG)**, Alexa Fluor 488-conjugated	Jackson ImmunoResearch	Cat#715-545-150	1:400	Immunofluorescence
Donkey polyclonal **anti-(Rabbit-IgG)**, Alexa Fluor 488-conjugated	Jackson ImmunoResearch	Cat#711-545-152	1:400	Immunofluorescence
Donkey polyclonal **anti-(Rat-IgG)**, Cy3-conjugated	Jackson ImmunoResearch	Cat#712-165-153	1:400	Immunofluorescence
Goat polyclonal **anti-(Mouse-IgG)**, Hrp-conjugated	Bio-Rad Laboratories, Hercules, CA, USA	Cat#5178-2504	1:20 000	Western blot
Goat polyclonal **anti-(Rabbit-IgG)**, Hrp-conjugated	Bio-Rad Laboratories	Cat#5196-2504	1:20 000	Western blot

Table S4. List of antibodies used in the present study. Host species, immunoreactive antigens, clone identifiers, commercial information, working dilutions and applications are listed for each of the antibodies used in this study.

Table S5

Instrument	Source	Application
SZX16 Stereomicroscope	Olympus, Hamburg, HH, Germany	Whole-mount imaging (Fig. 1A-C, 4A and S4)
Aperio ScanScope XT equipped with a 20x/0.75NA dry objective	Leica Biosystems, Nussloch, BW, Germany	FFPE tissue slide optical imaging (Fig. 2A-B and S1C)
SP8 Confocal Microscope, equipped with a 40x/1.3NA immersion oil objective	Leica Microsystems, Wetzlar, HE, Germany	FFPE tissue slide fluorescence confocal imaging (Fig. 2D and S1A)
BX61 Upright Wide Field Microscope, equipped with a 100x/1.35NA immersion oil objective	Olympus	Immunocytofluorescence imaging (Fig. 5A and S5)
DM6-B Microscope, equipped with a 63x/1.40NA or a 100x/1.40NA immersion oil objective	Leica Microsystems	Immunocytofluorescence imaging (Fig. S6A,C)
IX81 Inverted Fluorescence Automated Live cell Microscope, equipped with a 10X/0.4NA dry objective	Olympus	Time-lapse fluorescence imaging (Fig. 7D and S7C)
IX81 Inverted Fluorescence Automated Live cell Microscope, equipped with a 20X/0.45NA dry objective	Olympus	Time-lapse fluorescence imaging (Fig. 5C and S6B)
ECLIPSE Ti Inverted Microscope System, equipped with 20x/0.75NA dry objective	Nikon, Tokyo, Japan	Time-lapse fluorescence imaging (Fig. 5C and S6B)
THUNDER DMI8 Imager, equipped with a 20x/0.4NA dry objective	Leica Microsystems	Time-lapse fluorescence imaging (Fig. 5C and S6B)
DS-5Mc-U1 Digital Sight Camera	Nikon	Equipped on SZX16 Stereomicroscope
CoolSNAP EZ	Photometrics, Huntington Beach, CA, USA	Equipped on BX61 Upright Wide Field Microscope
Zyla 4.2 sCMOS	Andor Technology (Oxford Instruments), Belfast, Antrim, UK	Equipped on DM6-B Microscope and ECLIPSE Ti Inverted Microscope System
ORCA R-2 CCD Camera	Hamamatsu, Hamamatsu City, Japan	Equipped on IX81 Inverted Fluorescence Automated Live cell Microscope
ORCA-AG	Hamamatsu	Equipped on IX81 Inverted Fluorescence Automated Live cell Microscope
DFC9000 GTC	Leica Microsystems	Equipped on THUNDER DMI8 Imager
Cage incubator for live cell imaging	Oko-Lab, Ambridge, PA, USA	Equipped on time-lapse microscopes

Table S5. List of instruments used for image acquisition in the present study. Microscopes, cameras, objectives with magnifications and numerical apertures, commercial information, applications and references to figures are indicated for each of the imaging instruments used in this study.

Table S6

Gene symbol	Gene name	MGI ID	TaqMan® assay ID
18s (Rn18s)	18S ribosomal RNA	97943	Hs99999901_s1
Aldh1a1	Aldehyde dehydrogenase family 1, subfamily A1	1353450	Mm00657317_m1
Anapc5	Anaphase-promoting complex subunit 5	1929722	Mm00508066_m1
Anln	Anillin, actin binding protein	1920174	Mm00503748_m1
Aurka	Aurora kinase A	894678	Mm01248177_m1
Aurkb	Aurora kinase B	107168	Mm01718140_m1
Bub1	BUB1, mitotic checkpoint serine/threonine kinase	1100510	Mm00660135_m1
Bub1b	BUB1B, mitotic checkpoint serine/threonine kinase	1333889	Mm00437811_m1
Bub3	BUB3 mitotic checkpoint protein	1343463	Mm01275713_m1
Ccna2	Cyclin A2	108069	Mm00438064_m1
Ccnb1	Cyclin B1	88302	Mm00838401_g1
Ccnb2	Cyclin B2	88311	Mm00432351_m1
Ccnf	Cyclin F	102551	Mm00432385_m1
Cdc20	Cell division cycle 20	1859866	Mm00650983_g1
Cdca2	Cell division cycle associated 2	1919787	Mm00558459_m1
Cdk1	Cyclin-dependent kinase 1	88351	Mm00772471_m1
Cdk2	Cyclin-dependent kinase 2	104772	Mm00443947_m1
Cenpe	Centromere protein E	1098230	Mm00620549_m1
Chek1	Checkpoint kinase 1	1202065	Mm01176757_m1
Haus2	HAUS augmin-like complex, subunit 2	1913546	Mm00508375_m1
Incenp	Inner centromere protein	1313288	Mm01198109_m1
Kif20a	Kinesin family member 20A	1201682	Mm00436226_m1
Kif2c	Kinesin family member 2C	1921054	Mm00728630_s1
LGN (Gpsm2)	G-protein signalling modulator 2	1923373	Mm01195154_m1
Mad2l1	MAD2 mitotic arrest deficient-like 1	1860374	Mm00786984_s1
mInsc (Insc)	INSC spindle orientation adaptor protein	1917942	Mm00620583_m1
Mis12	MIS12 kinetochore complex component	1914389	Mm00508986_m1
Mphosph8	M-phase phosphoprotein 8	1922589	Mm00470131_m1
Ncapd2	Non-SMC condensin I complex, subunit D2	1915548	Mm00514073_m1
NuMA (Numa1)	Nuclear mitotic apparatus protein 1	2443665	Mm00659817_m1
Numb	NUMB endocytic adaptor protein	107423	Mm00477927_m1
Par3 (Pard3)	Par-3 family cell polarity regulator	2135608	Mm00473929_m1
Par6 (Pard6a)	Par-6 family cell polarity regulator alpha	1927223	Mm00480004_m1
Plk1	Polo like kinase 1	97621	Mm00440924_g1
Plk4	Polo like kinase 4	101783	Mm00550358_m1
Rpl13a	Ribosomal protein L13A	1351455	Mm05910660_g1
Rpl9	Ribosomal protein L9	1298373	Mm00834201_g1
Smc4	Structural maintenance of chromosomes 4	1917349	Mm00713073_m1
Spag5 (Astrin)	Sperm associated antigen 5	1927470	Mm00840133_m1
Top2a	Topoisomerase (DNA) II alpha	98790	Mm00495703_m1

Table S6. List of genes analyzed by qRT-PCR in the present study. Gene symbols, gene names, Mouse Genome Informatics gene IDs and Taqman® assay IDs are indicated for each of the genes analyzed in this study.

Supplementary Datasets

Dataset 1, Dataset 2 and Dataset 3 are provided in Excel format.

Dataset 1. List of gene sets used for Gene Set Enrichment Analysis (30) of aged p66Shc-/- *vs* WT mammosphere gene expression levels. Datasets were either downloaded from MSigDB collections, or manually curated from already published data (31-35). Human orthologs of mouse genes were obtained using the g:Orth (Orthology Research) tool (70).

Dataset 2. List of mammary stem cell (MaSC)-genes differentially expressed in p66Shc-/- *vs* WT aged mammospheres, analyzed by RNA-sequencing. Genes listed here were categorized as "MaSC-markers" if satisfying one of the two following criteria: *i)* being present in at least 3 out of 5 datasets of genes upregulated in MaSCs (31-35), and/or *ii)* being object of a previously published functional study. Human and mouse gene symbols, along with literature references, gene expression fold changes and false discovery rates (FDR) are indicated.

Dataset 3. List of cell polarity-genes differentially expressed in p66Shc-/- *vs* WT aged mammospheres, analyzed by RNA-sequencing. Genes listed here were categorized as "cell polarity- or asymmetric division-markers" if object of a functional or descriptive study in vertebrates. Human and mouse gene symbols, along with literature references, gene expression fold changes and false discovery rates (FDR) are indicated.

Original Data

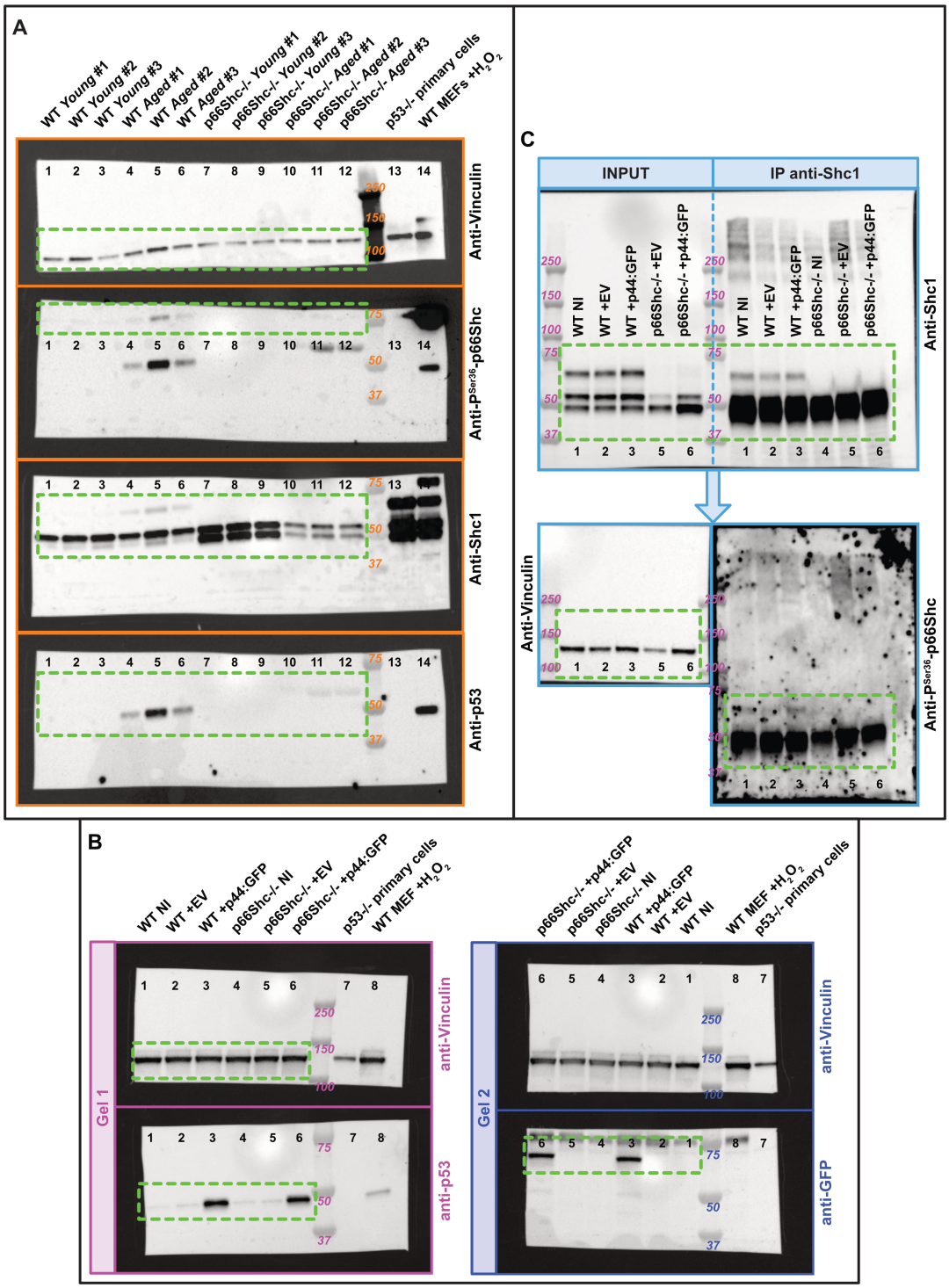

Original Data. Uncropped western blot images. **(A)** Appendix to Fig. 6A. **(B)** Appendix to Fig. S7A. **(C)** Appendix to Fig. S7B. In (A-C), colorimetric and chemiluminescent images of membranes were digitally acquired with a ChemiDoc XRS$^+$ instrument and merged using Image Lab software (Bio-Rad Laboratories); cropped areas are shown by green dashed lines; lane numbering, sample names, antibodies used and molecular weights of the protein marker bands are indicated.